Chemistry and *P-V-T* equation of state of FeO_2H_x at the base of Earth's lower mantle and their geophysical implications

Ruilian Tang[1,2*], Jin Liu[1], Duck Young Kim[1], Ho-kwang Mao[1], Qingyang Hu[1], Bin Yang[1], Yan Li[3], Chris J. Pickard[4,5] Richard J. Needs[6], Yu He[1,7], Haozhe Liu[1], Vitali Prakapenka[8], Yue Meng[9], Jinyuan Yan[10]

[1]Center for High Pressure Science and Technology Advanced Research, Changchun, 130012, China.
[2]School of Materials Science and Engineering, Changchun University of Science and Technology, Changchun, 130022, China
[3]State Key Laboratory of Superhard Materials, College of Physics, Jilin University, Changchun, 130012, China.
[4]Department of Materials Science and Metallurgy, University of Cambridge, Cambridge Cb3 0Fs, United Kingdom
[5]Advanced Institute for Materials Research, Tohoku University, Sendai, 980-8577, Japan
[6]Theory of Condensed Matter Group, Cavendish Laboratory, Cambridge CB3 0HE, United Kingdom
[7]Key Laboratory of High-Temperature and High-Pressure Study of the Earth's Interior, Institute of Geochemistry, Chinese Academy of Sciences, Guiyang, Guizhou 550081, China
[8]Center for Advanced Radiation Sources, University of Chicago, Chicago, IL, USA.
[9]Advanced Photon Source, Argonne National Laboratory, Argonne, IL 60439, USA.
[10]Advanced Light Source, Lawrence Berkeley National Laboratory, Berkeley, CA 94720, USA.

*ruilian.tang@hpstar.ac.cn, +86 151 6436 9228

The hydrogen-absorbing ability of a mantle mineral in its structure determines the capacity of the water reservoirs hosted by the mineral. Water reservoirs at the base of Earth's mantle directly influence the fate of water brought down by slab subduction and the seismic heterogeneity such as ultralow-velocity zones (ULVZs) at the core-mantle boundary. Pyrite-FeO_2H_x ($0 \leq x \leq 1$) presents a possibility of such reservoirs in the deep mantle [1-3]. Ever since the discovery of this mineral phase, however, its chemistry at the lower mantle conditions has been debated [1, 2]. We conducted kinetics experiments of pyrite-FeO_2H_x dehydrogenation at 110 GPa/2100 K, 110 GPa/2300 K, and 120 GPa/2300 K and *P-V-T* equation of state analysis using *in situ* synchrotron x-ray diffraction. We found that *x* approaches 0.80, 0.75, and 0.79, respectively, at the above conditions. The collective *P-V-T* data yield K_0 = 241(13) GPa, K' = 4.2(4), dK/dT = -0.028(1) GPa/K, α_0 = 4.32(13)×10^{-5} K^{-1}, and α_1 = 0.31(10)×10^{-8} K^{-2} for the composition of x = 0.75±0.04. Our first-principles calculations indicate that $FeO_2H_{0.75}$ with a slightly distorted pyrite structure is stable at 100 GPa. These results indicate that this mineral is likely present in the deep mantle with rather a partially dehydrogenated composition than FeO_2 or FeOOH. The results also clarify the difference between the ULVZs originated from pyrite-FeO_2H_x and those from partial melting in terms of shear and compressional wave seismic velocity reduction ratio $\delta \ln V_S / \delta \ln V_P$.

Three sequences of time-resolved kinetics experiments using laser-heated diamond anvil cell (LHDAC) and synchrotron x-ray diffraction were conducted at 110 GPa/2100 K, 110 GPa/2300 K, and 120 GPa/2300 K for 9, 12, and 7 hours, respectively. Experimental details are given in the **Supplementary Data**. The hydrogen concentration (*x*) in pyrite-FeO_2H_x is determined by comparing the cell volume of the sample after it was quenched to room temperature with those of the end members (FeOOH and FeO_2) at the same pressure, *i.e.*, $x = (V_{obs}-V_{FeO2})/\Delta V_H$, in which V_{obs} and V_{FeO2} are unit cell volumes of FeO_2H_x and end member FeO_2, respectively, and ΔV_H is a predetermined volume expansion due to a single formula unit of hydrogen ($V_{FeOOH} - V_{FeO2}$) [4]. As shown in Fig. 1a, the obtained *x* values as a function of the heating duration were fit based on the first-order reaction equation dx/dt = -kx (where k is a time-independent constant for a given environment) for the dehydrogenation: FeOOH = FeO_2H_x + ½(1-x)H_2. We found that *x* approaches 0.80, 0.75, and 0.79 in the samples at 110 GPa/2100 K, 110 GPa/2300 K, and 120 GPa/2300 K conditions, respectively, as the time approaches infinity (equilibrium). These results indicate that pyrite-FeOOH loses hydrogen through a dehydrogenation process to approach an equilibrium state at the pressure and temperature conditions in the deep lower mantle, and a part of hydrogen remains in the equilibrium state. As shown in Fig. 1a, the amount of the remaining hydrogen decreases with increasing temperature (*i.e.* 0.80 at 110 GPa/2100 K to 0.75 at 110 GPa/2300 K), which agrees with the observation of temperature-enhanced dehydrogenation by Hu *et al*. [4], whereas pressure increases the amount of the remaining hydrogen (*i.e.* 0.75 at 110 GPa/2300 K to 0.79 at 120 GPa/2300 K). We selected the *in situ P-V-T* data for the composition of pyrite-$FeO_2H_{0.75\pm0.04}$ from previously published data and our current study, and fit them to the high-temperature 3rd-order Birch-Murnaghan EoS (Fig. 1b) yielding V_0 = 108.9(1) Å^3, K_0 = 241(13) GPa, K' = 4.2(4), dK/dT = -0.028(1) GPa/K, α_0 = 4.32(13)×10^{-5} K^{-1}, and α_1 = 0.31(10)×10^{-8} K^{-2}.

To verify the stability of the partially dehydrogenated pyrite-FeO_2H_x phase, we conducted a crystal structure search in the Fe-O-H ternary system at 100 GPa using the Ab Initio Random Structure Searching (AIRSS) method (see **Supplementary Data**) with the focus on dehydration along FeO_2- FeO_2H. We found that $FeO_2H_{0.75}$ with a slightly distorted

pyrite structure becomes a ground state in the FeO_2-FeO_2H system (Fig. 1c) and its calculated phonon dispersion relations exhibit dynamical stability (Fig. 1d). The distorted structure deviates from the cubic structure by 0.39 degrees in the lattice angle, possessing a rhombohedral unit cell with a space group of *R-3*. Our computation of the structure relaxation for the distorted pyrite-$FeO_2H_{0.75}$ yields a bulk modulus of K_0=248.2 GPa and its pressure derivative K'=3.81 with V_0=109.6 Å^3. These values are consistent with the above experimental result within the uncertianty and the tendency of trade-off between K_0 and K'.

Our experimental results on the dehydrogenation kinetics (Fig. 1a) indicate that the on-site chemistry of pyrite-FeO_2H_x is a function of pressure, temperature, and the *P-T* history of the sample. The dehydrogenation process may take hours to reach equilibrium. Therefore, *in situ* x-ray diffraction data may show a large variation in the hydrogen concentration of the sample within this period, depending on the duration of heating and the P/T history that the sample has experienced. This kinetics result explains the scattering *x* values in the literature [1-4] and is consistent with the general trend of lower *x* values at higher temperatures or lower pressure [4].

The thermodynamically stable state with a large remaining fraction of hydrogen in the pyrite-FeO_2H_x phase makes a large water reservoir possible in the deep lower mantle. Taking into account the pressure and temperature influences on the equilibrium composition, the pyrite-FeO_2H_x (if stable, see **Supplementary Data**) may still remain hydrogen concentration close to $x = 0.7\pm0.1$. This is equivalent to 7±1 wt.% water storage capability. Based on the derived EoS, pyrite-FeO_2H_x (x=0.75±0.04) in the lower mantle is about 24% denser (Fig. 1a) than the surrounding mantle of the Preliminary Reference Earth Model (PREM). When water (hydrogen) in the subduction slab meets the hot iron at the core-mantle boundary (CMB), the reaction $4Fe+2H_2O=FeO_2H_x+3FeH_{(4-x)/3}$ may pass a portion of the hydrogen into the FeO_2H_x water reservoir in the lower mantle and incorporate the rest into the outer core through iron hydride [3, 5]. Previous experiments have also demonstrated that metallic iron may be present in the uppermost lower mantle due to charge disproportionation $3Fe^{2+}\rightarrow 2Fe^{3+}+Fe^0$ caused by the increase of Fe^{3+} in Al-bearing bridgmanite [6]. Observations of a metallic iron phase in the inclusions of natural diamonds that presumably originate from the top of the lower mantle [7] support this speculation from the high-pressure experiments. Such an increase of Fe^{3+} in Al-bearing bridgmanite was recently reported in the pressure range from 60 to 80 GPa [8], indicating a possible charge disproportionation in the mid-depth of the lower mantle. If dehydration melting of phase δ-H solid solutions happens in this depth range, as expected in peridotite system [3], reactions between the metallic iron and the hydrous melt will pass hydrogen to FeO_2H_x and iron hydride at these depths, which will sink to the bottom of the lower mantle. Either formed at the mid-depth of the lower mantle or at the CMB, FeO_2H_x may promote the water cycling down in the lower mantle and retain water at the bottom of the lower mantle as a water reservoir [3].

We converted the experimental isothermal bulk modulus (K_T) to adiabatic bulk moduli (K_s) using $K_s = (1 + \alpha\gamma T)K_T$ (γ: Grüneisen parameter and α: thermal expansion coefficient), and calculated the shear modulus using $G = (3/2)(1-2\nu)/(1+\nu)K$ (ν: Poisson's ratio). We adopted the value of ν measured at 133 GPa and 300 K using nuclear resonant inelastic X-ray scattering (NRIXS) and extroplated to high temperatures based on first-principles calculations [9]. The derived seismic velocities of the P-wave (V_P) and S-wave (V_S) in pyrite-$FeO_2H_{0.75\pm0.04}$ along the geotherm of the lower mantle are derived as shown in Fig.

2a. While the density of pyrite-$FeO_2H_{0.75\pm0.04}$ is about 24% higher than the surrounding mantle of PREM, the V_P and V_S are 23% and 44% slower than the PREM, respectively, at the bottom of the lower mantle. These results derived from our *P-V-T* experiment data are consistent with the extrapolation of the nuclear resonant inelastic x-ray scattering (NRIXS) result at 130 GPa and room temperature (x = 0.72 calculated using this the method of this study) [9]. Fig. 2b shows influences of the volume fraction of pyrite-$FeO_2H_{0.75\pm0.04}$ in the mantle on the bulk density, V_P, and V_S, calculated using Voigt-Reuss-Hill average, at the bottom of the lower mantle. Mixing pyrite-$FeO_2H_{0.75\pm0.04}$ with ambient mantle produces a seismic velocity reduction with a shear-wave to compressional-wave ratio of $\delta\ln V_S/\delta\ln V_P$=2:1. This is a distinct feature in contrast to that of partial melting, which is believed to reduce seismic velocities along $\delta\ln V_S/\delta\ln V_P$=3:1 [10] due to its highly differentiated influences on shear and compressional waves. For comparison, the $\delta\ln V_S/\delta\ln V_P$=3:1 line is also plotted in Fig. 2b (red broken line). This feature will help seismologists to differentiate possible origins of ULVZs.

We surveyed reported ULVZs around the large low-shear-velocity-province (LLSVP) beneath the Pacific. As shown in Fig. 2c, most of the ULVZs inside the LLSVP show a $\delta\ln V_S/\delta\ln V_P$=3:1 seismic velocity reduction. A few studies, however, reported some distinct ULVZs near the margins of the LLSVP. Hutko *et al.* [11] analyzed an extensive, high-quality P-wave data set comprising of short-period and broadband signals using regional one-dimensional double-array stacking/modeling with reflectivity synthetics. They found that by retaining only events with stable PcP energy in the final data stacks yielded reductions of V_S and V_P ranging from -6% to -8% (±2-3%) and -3% to -4% (±1%), respectively, for the ULVZ at the northern border of the LLSVP (purple oval at about 9°N and 151°W in Fig. 5), matching $\delta\ln V_S/\delta\ln V_P$=2:1 nicely. Based on such a low $\delta\ln V_S/\delta\ln V_P$ ratio, they inferred that the ULVZ has less connectivity of melt than those inside the LLSVP. Avants *et al.* [12] compared their modeling of precursors to the tangential-components of core-reflected ScS phases with the analogous modeling of PcP precursors for the same region. They also suggested that an alternative mechanism other than partial melting is responsible for the ULVZ at the northern boundary of the LLSVP based on the estimated $\delta\ln V_S/\delta\ln V_P$ value close to 2:1 for two of three bins in their dataset. Although some other solid phases such as iron-rich post-perovskite and iron-enriched oxides (magnesium wüstite) have also been reported to possibly give rise to a ULVZ, mixing the former with ambient mantle of PREM produces a reduction of V_S and V_P along $\delta\ln V_S/\delta\ln V_P$ = 3.5~4 and the latter produces $\delta\ln V_S/\delta\ln V_P$ = 1.2~1.5 [13]. In addition, the location of the above-mentioned ULVZs at the boundaries of the LLSVP indicate that these ULZVs with $\delta\ln V_S/\delta\ln V_P$=2:1 preferably occur at relatively low-temperature zones, which may be justified by the possible instability of FeO_2H_x at higher temperatures [2]. Not only the $\delta\ln V_S$ and $\delta\ln V_P$ values, but also the density elevation $\delta\ln\rho$ (~3%) from Hutko *et al.* [11] consistently yield 10% to 13% volumetric fractions of pyrite-FeO_2H_x (Fig. 5) responsible for the origin of this "low-temperature" ULVZ. Therefore, these seismic observations favor the presence of a FeO_2H_x water reservoir in the relatively low-temperature zones.

Whether the FeO_2H_x water reservoir survives or not at the base of the lower mantle largely depends on its thermal stability. Presence of pyrite-FeO_2H_x is reported in the experiment at 3100-3300 K and 125 GPa [9]. This is so far the highest temperature that pyrite-FeO_2H_x reportedly survives. On the other hand, experimental observation of Fe_2O_3 post-perovskite was reported to coexist with pyrite-FeO_2H_x after heating pyrite-FeO_2H_x above 2400 K [2], indicating pyrite-FeO_2H_x may become unstable above this temperature.

In the hydrous mantle mass of magnesium silicate and oxides system ($MgO–Al_2O_3–Fe_2O_3–SiO_2–H_2O$), pyrite-$FeO_2H_x$ was experimentally observed coexisting with post-perovskite and iron-bearing δ-phase at temperatures below 2400 K and pressures of the base of the lower mantle [14]. Further studies are needed to fully understand its thermal stability at the base of the lower mantle. But the current experimental observations have evidenced the stability of pyrite-FeO_2H_x at least in the cold regions near the subduction slabs that reach the bottom of the lower mantle [3, 9]. When the mantle convection brings pyrite-FeO_2H_x piles from cold regions to a hot region where they become unstable, the decomposition, $2FeO_2H_x = Fe_2O_3 + xH_2O + 1/2\ (1 - x)O_2$, may release water and oxygen (for $x < 1$). The released water will eventually cycle back to the surface along mantle plumes. If large amounts of pyrite-FeO_2H_x accumulate before they decompose, an eruption of such decompositions could be linked to the Great Oxidation Event [5].

Conflict of interest: The authors declare that they have no conflict of interest.

Acknowledgments: We would like to thank Dr. Eran Greenburg and Dr. Sergey Tkachev at GeoSoilEnviroCARS (GSECARS) for their technical support. Portions of this work were performed at GSECARS (Sector 13) and HPCAT (Sector 16), Advanced Photon Source (APS), Argonne National Laboratory. Use of the COMPRES-GSECARS gas loading system was supported by COMPRES under NSF Cooperative Agreement EAR - 1606856 and by GSECARS through NSF grant EAR-1634415 and DOE grant DE-FG02-94ER14466. HPCAT operations are supported by DOE-NNSA's Office of Experimental Sciences. APS is supported by DOE-BES, under contract no. DE-AC02-06CH11357. This research also used resources of the Advanced Light Source, which is a DOE Office of Science User Facility under contract no. DE-AC02-05CH11231. RT acknowledges the support of the Youth Science Foundation of Changchun University of Science and Technology (No. XQNJJ-2018-15). Portions of this research were supported by the NSAF Grant No. U1530402. HKM is supported by NSF Grants EAR-1722515 and EAR-1447438. DYK acknowledges the support by the NSFC (Grant No. 11774015). CJP is supported by the Royal Society through a Royal Society Wolfson Research Merit award and the EPSRC through Grants No. EP/P022596/1.

Author Contributions: R.T and H.-K.M. conceived and supervised the project; R.T and J.L. conducted the synchrotron XRD measurements; D.K., C.J.P. R.J.N. and Y.H. conducted theoretical calculations; Q.H., H.L., Y.L., V.B.P., Y.M. and J.Y. assisted with the techniques at the synchrotron beamlines; R.T., B.Y. and Y.L. prepared the DAC cells and samples. R.T. performed the analysis; R.T. and H.-K.M. wrote the manuscript in consultation with all coauthors.

References

[1] Hu Q, Kim DY, Yang W, et al. FeO_2 and FeOOH under deep lower-mantle conditions and earth's oxygen-hydrogen cycles. Nature, 2016, 534: 241-244.
[2] Nishi M, Kuwayama Y, Tsuchiya J, et al. The pyrite-type high-pressure form of FeOOH. Nature, 2017, 547: 205-208.
[3] Yuan L, Ohtani E, Ikuta D, et al. Chemical reactions between Fe and H_2O up to megabar pressures and implications for water storage in the earth's mantle and core. Geophysical Research Letters, 2018, 45: 1330-1338.

[4] Hu Q, Kim DY, Liu J, et al. Dehydrogenation of goethite in earth's deep lower mantle. Proceedings of the National Academy of Sciences, 2017, 114: 1498-1501.
[5] Mao H-K, Hu Q, Yang L, et al. When water meets iron at earth's core–mantle boundary. National Science Review, 2017, 4: 870-878.
[6] Frost DJ, Liebske C, Langenhorst F, et al. Experimental evidence for the existence of iron-rich metal in the earth's lower mantle. Nature, 2004, 428: 409-412.
[7] Smith EM, Shirey SB, Nestola F, et al. Large gem diamonds from metallic liquid in earth's deep mantle. Science, 2016, 354: 1403-1405.
[8] Shim S-H, Grocholski B, Ye Y, et al. Stability of ferrous-iron-rich bridgmanite under reducing midmantle conditions. Proceedings of the National Academy of Sciences, 2017, 114: 6468-6473.
[9] Liu J, Hu Q, Young Kim D, et al. Hydrogen-bearing iron peroxide and the origin of ultralow-velocity zones. Nature, 2017, 551: 494-497.
[10] Williams Q, Garnero EJ. Seismic evidence for partial melt at the base of earth's mantle. Science, 1996, 273: 1528-1530.
[11] Hutko AR, Lay T, Revenaugh J. Localized double-array stacking analysis of PcP: D″ and UVLZ structure beneath the Cocos plate, Mexico, central Pacific, and north Pacific. Physics of the Earth and Planetary Interiors, 2009, 173: 60-74.
[12] Avants M, Lay T, Garnero EJ. A new probe of ULVZs-wave velocity structure: Array stacking of ScS waveforms. Geophysical Research Letters, 2006, 33: L07314.
[13] Chen J. Tracking the origin of ultralow velocity zones at the base of earth's mantle. National Science Review, 2021, nwaa308.
[14] Yuan H, Zhang L, Ohtani E, et al. Stability of fe-bearing hydrous phases and element partitioning in the system $MgO–Al_2O_3–Fe_2O_3–SiO_2–H_2O$ in earth's lowermost mantle. Earth and Planetary Science Letters, 2019, 524: 115714.

Figure captions:

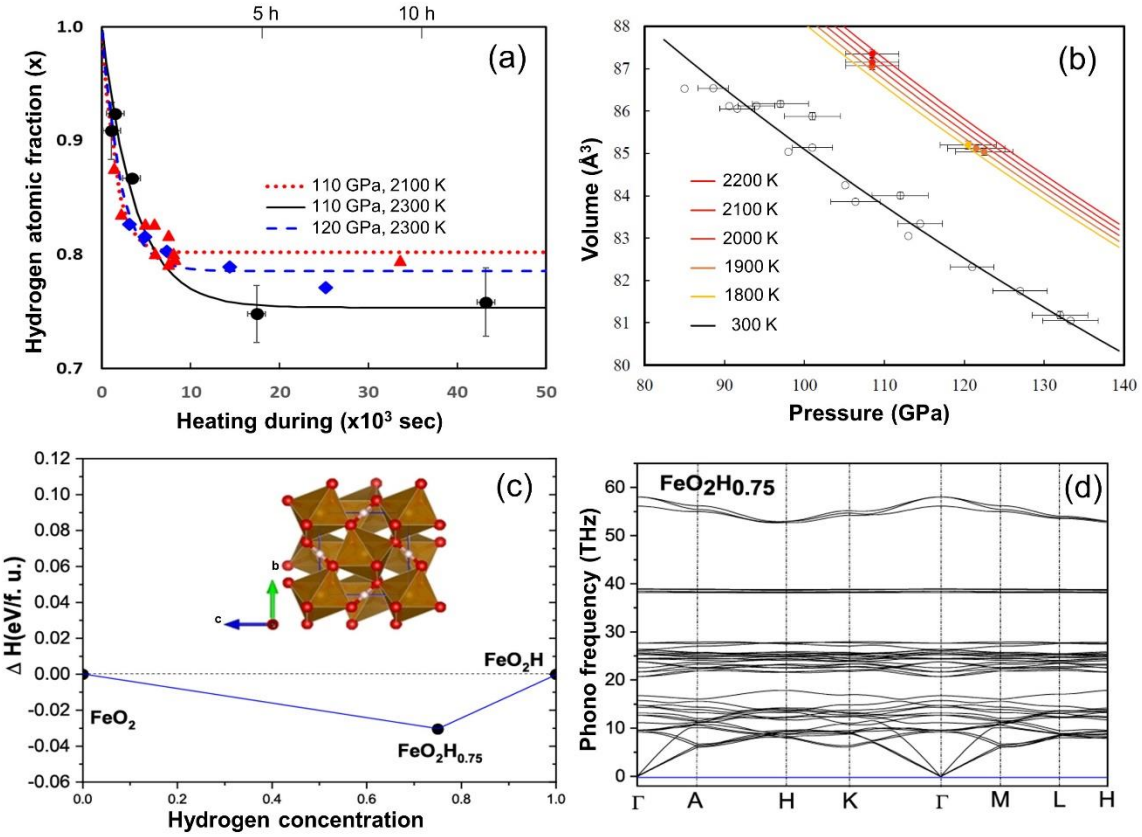

Fig. 1. (a) Derived hydrogen atomic fraction *x* in pyrite-FeO_2H_x as a function of heating duration at the indicated pressure and temperature conditions, (b) The *P-V-T* data of pyrite-$FeO_2H_{0.75\pm0.04}$, (c) The calculated convex hull along FeO_2 and FeO_2H, (d) Phonon dispersion relations of $FeO_2H_{0.75}$ showing its dynamics stability. Fittings to the first-order reaction equation are presented by the different lines for the data symbols of the corresponding colors in (a). Bars attached to the symbols in (a) and (b) represent estimated experimental errors. The *P-V-T* data in (b) are from this study (open circles with both horizontal and vertical error bars, and solid circles), Liu *et al.* 2017 [9] (open circles with horizontal error bar) and Hu *et al.* 2017 [4] (open circles without error bar). The solid lines are fittings to the third-order Birch-Murnaghan EoS at the indicated temperatures. The inset in (c) shows the structure of the intermediate ground-state $FeO_2H_{0.75}$ (a distorted pyrite structure, space group: *R-3*).

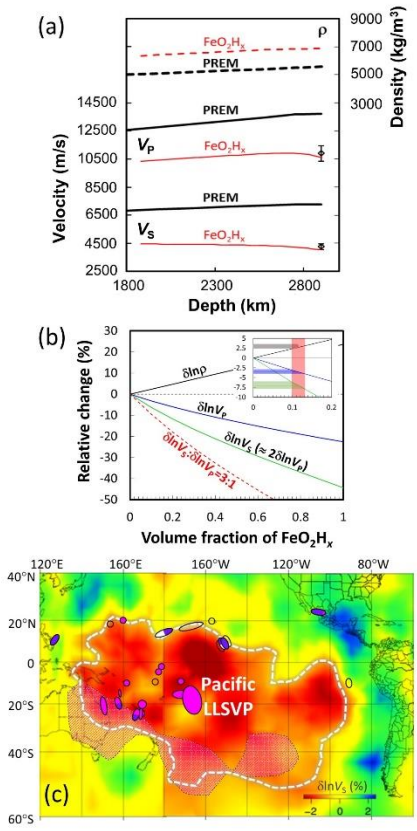

Fig. 2. (a) Density (ρ), compressional wave velocity (V_P) and shear wave velocity (V_S) in pyrite-FeO_2H_x (x=0.75±0.04) along the lower-mantle geotherm, (b) The relative changes δlnρ, δlnV_S and δlnV_P as a function of volumetric fraction of pyrite-FeO_2H_x mixing with ambient mantle at the bottom of the lower mantle, (c) The δlnV_S to δlnV_P ratio and their locations of the ULVZs beneath the Pacific and nearby. For comparison, PREM (bold lines) and extrapolations of the velocities from NRIXS experimental data [5] (x = 0.72) at 130 GPa and room temperature to the conditions of the bottom of the lower mantle (diamonds) are also plotted in (a). The red broken line in (b) shows the expected δlnV_S with δlnV_S:δlnV_P =3:1 (a typical feature for partial melting) for comparison. The inset in (b) shows the values of δlnρ, δlnV_P, and δlnV_S (horizontal shades) of the ULVZ at the northern margin of the LLSVP beneath the Pacific reported by Hutko *et al* l[11]. Circles/ovals in pink, magenta, white, or transparent in (c) represent the detected ULVZs with δlnV_S/δlnV_P = 3:1, 2:1, 1:1, or undetermined, and the shaded patch indicates the area with a high ULVZ likelihood. The background is the tomography based on the shear velocity model GyPSuM at a 2800 km depth, and the white contour represents the -0.4% δlnV_P boundary of the LLSVP**.**